coatings

MDPI

Supplementary Materials

The Role of Anodising Parameters in the Performance of Bare and Coated Aerospace Anodic Oxide Films

Mariana Paz Martinez-Viademonte [1,2,*], Shoshan T. Abrahami [3], Meisam D. Havigh [1], Kristof Marcoen [1], Theodor Hack [2], Malte Burchardt [4] and Herman Terryn [1]

[1] Research Group, Electrochemical and Surface Engineering (SURF), Department of Materials and Chemistry, Vrije Universiteit Brussel, Pleinlaan 2, 1050 Brussels, Belgium; meisam.dabiri.havigh@vub.be (M.D.H.); kristof.marcoen@vub.be (K.M.); herman.terryn@vub.be (H.T.)

[2] Airbus Central Research and Technology, Willy-Messerschmitt-Straße 1, 82024 Taufkirchen, Germany; theo.hack@airbus.com

[3] Department of Materials Science and Engineering, Delft University of Technology, Mekelweg 2, 2628 CD Delft, The Netherlands; s.t.abrahami@tudelft.nl

[4] Airbus Operations GmbH Deutschland, GmbH, Airbus Allee. 1, 28199 Bremen, Germany; malte.burchardt@airbus.com

* Correspondence: mariana.paz@airbus.com

1. Oxide Chemistry Characterisation: Experimental

1.1. X-Ray Photoelectron Spectroscopy

Detailed spectra for the C1s, O1s, Al2p and S2p have been measured for both porous and barrier oxide films. High-resolution spectra were obtained using pass-energy of 26 eV and a step size of 0.5 eV. For barrier oxide films, a second set of high-resolution spectra were acquired keeping all parameters constant except for the take-off angle, which was reduced to 15°. The data obtained at this take-off angle corresponds to the near-surface concentration of the film, allowing to study the outer region of the film.

Finally, a mild sputtering using an argon cluster ion gun has been performed to remove the contamination layer on the surface of barrier oxide films (8 cycles of 30 s in a 3 × 3 μm^2 area and a 500 V accelerating voltage). Furthermore, an in-depth chemical composition profile of barrier oxide films has been acquired (35 cycles of 1 minute in a 3 × 3 μm^2 area and a 1 kV accelerating voltage).

1.2. Time-of-Flight Secondary Ion Mass Spectrometry (ToF-SIMS)

ToF-SIMS analysis has been performed with a TOF.SIMS 5 system from IONTOF (Münster, Germany), using a 30 keV Bi_3^+ primary ion beam which is operated in high current bunched mode for high mass resolution (approximately 8000 at 29 m/z ($^{29}Si^+$)). The lateral resolution is estimated to be 3 μm and the target current is 0.7 pA. For each measurement, an analysis raster of 500 μm × 500 μm was chosen. The analysis time is limited such that the primary ion dose is kept below the static limit of 1×10^{13} ions cm^{-2} $analysis^{-1}$.

2. Oxide Chemistry Characterisation: Results

2.1. Oxide chemistry characterisation by XPS

2.1.1. XPS Characterisation of barrier anodic oxide films

Detailed spectra of the main detected elements, namely O, Al, C, S and F, was measured at two different take-off angles. Based on these spectra, the chemical compositions of barrier oxide films for 45° and 15° take-off angles were calculated. The results of these calculations are shown in Table S1. All oxides have similar chemical compositions, with an oxygen content of approximately 50%, and aluminium content of ca. 25%. The carbon content ranges between 15–17% for the measurements obtained at a 45° take-off angle and increases to 17–23% if measured at a smaller take-off angle. The variation of the carbon content with take-off angle indicates that the carbon signal comes from the adventitious

contamination layer on top of the barrier oxide film, since the carbon concentration decreases for larger take-off angles, when the probing depth increases and consequently the contribution of the contamination layer becomes less relevant. Moreover, even though tartaric acid is an organic acid and, as a consequence, it could be expected to see differences in the carbon concentration between the anodic oxides formed in the presence or absence of tartaric acid, no trend in this direction can be derived. The amount of carbon measured is similar for all oxides, regardless of the nature of the anodising electrolyte (SAA/TSA/T$^+$SA). Finally, a small fraction of fluoride and sulfur are detected. Fluoride (1–4%) is most likely coming from the pre-treatment, as it is present in the acidic pickling solution, while sulfur (0.5–2%) is incorporated from the anodising electrolyte into the oxide film.

Table S1. Chemical composition measured by XPS on barrier oxide layers at 45° and 15° take-off angles.

		Chemical composition [At.%]									
Oxide	**Take-Off Angle**	**C1s**	**σ**	**O1s**	**σ**	**F1s**	**σ**	**Al2p**	**σ**	**S2p**	**σ**
SAA 45 °C	45°	15.2	2.0	52.1	1.1	3.5	0.2	28.4	0.9	0.9	0.0
SAA 45 °C	15°	17.4	1.5	50.2	1.2	3.6	0.3	28.1	0.5	0.7	0.0
SAA 37 °C	45°	16.2	1.1	51.6	0.4	3.9	0.0	26.9	0.7	1.3	0.1
SAA 37 °C	15°	20.5	0.4	48.2	0.3	4.1	0.1	25.8	0.4	1.3	0.2
TSA 55 °C	45°	13.7	1.5	55.7	0.4	2.5	0.3	26.3	0.9	1.8	0.1
TSA 55 °C	15°	16.0	1.1	53.4	0.4	2.7	0.4	26.0	0.7	2.0	0.1
TSA 37 °C	45°	17.2	1.3	50.9	0.3	3.9	0.5	26.8	1.2	1.2	0.2
TSA 37 °C	15°	23.1	0.5	46.4	1.1	4.1	0.4	25.1	0.7	1.3	0.2
T$^+$SA 55 °C	45°	17.7	2.7	51.1	1.2	2.9	0.5	16.0	1.1	0.6	0.1
T$^+$SA 55 °C	15°	21.7	2.1	48.0	1.1	3.0	0.4	26.7	0.8	0.6	0.2
T$^+$SA 37 °C	45°	15.8	1.6	55.4	0.5	1.1	0.2	26.5	1.0	1.2	0.1
T$^+$SA 37 °C	15°	18.7	0.9	52.3	0.1	1.6	0.2	26.5	0.7	1.0	0.0

Detailed XPS spectra of the C1s and O1s regions measured at a 45° takeoff angle is provided in Figure S1. Again, no significant changes in the shape of the photoelectron peaks are visible among oxides, other than differences in intensity of the signal due to variations in the thickness of the adventitious contamination layer.

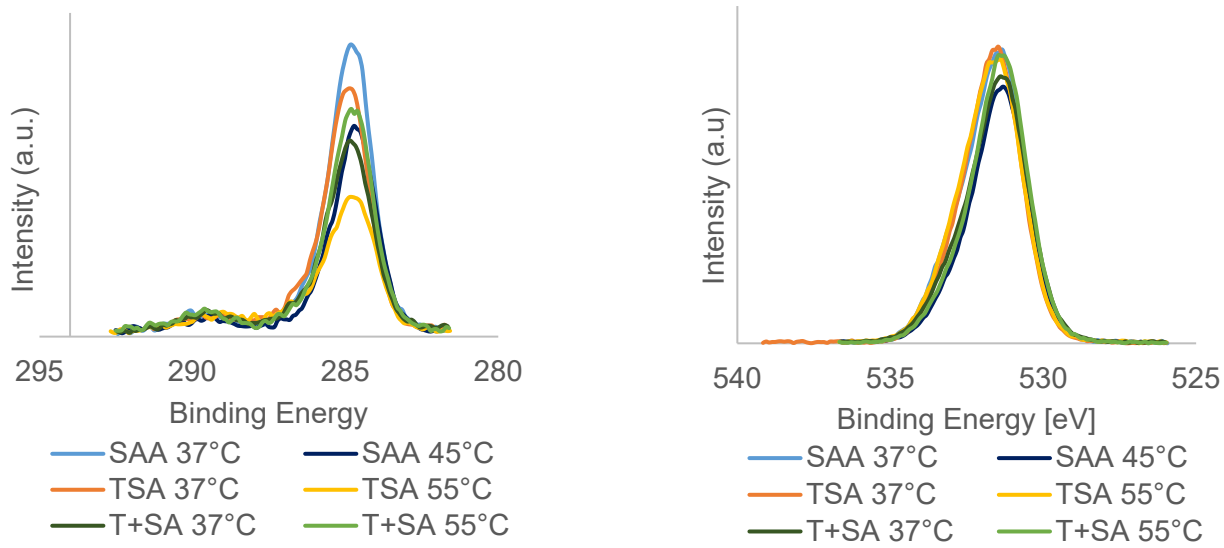

Figure S1. Detailed photoelectron peak for (**a**) C1s and (**b**) O1s.

These detailed spectra were deconvoluted into the common contributions. In particular, for the C1s the C–C, –OCO, and –CO contributions were considered. For the O1s peak, the contributions considered were $–O^{2–}$, $–OH^{–}$ and $–H_2O$. The constraints used for the fitting of the spectra were the ones proposed by Abrahami et al. [1] for similar systems (barrier anodic oxide films on aluminium substrates) and are summarised in Table S2. Figure S2 shows an example of the C1s and O1s fitted spectrum. To quantify the goodness of the fit the $\chi 2$ parameter is considered: the $\chi 2$ parameter for the fit of the O1s peak is in all cases below 2 and below 0.6 for the fit of the C1s peak.

Table S2. Constraints applied for the curve fitting of the O1s and C1s photoelectron peaks as proposed by Abrahami et al. [1].

C1s			O1s		
	FWHM [eV]	**Position lock [eV]**		**FWHM [eV]**	**Position lock [eV]**
C–C	1.6	0	$O^{2–}$	1.80–1.84	0
CO	2.0	1.5	$OH^{–}$	1.68–1.72	1.1–1.4
OCO	1.4–2.0	3.8–4.8	H_2O	2.03–2.07	2.43

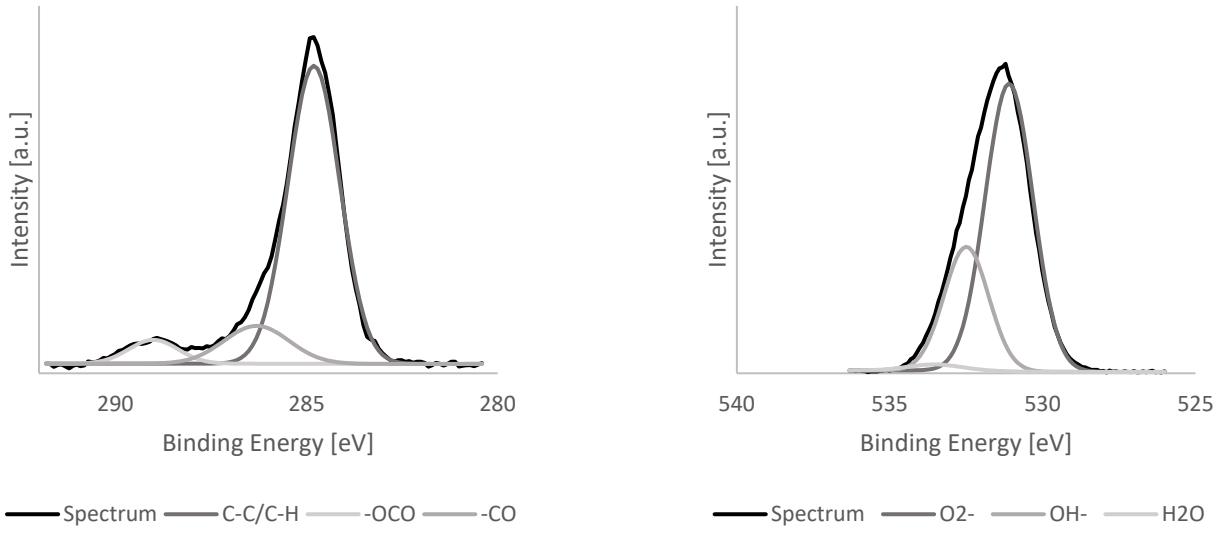

(**a**) (**b**)

Figure S2. Example of fitted photoelectron peak for (**a**) C1s and (**b**) O1s.

The results obtained from the fitting of the C1s and O1s spectra are summarized in Table S3. All studied conditions yield similar contribution of each particular chemical state, both for the C1s as for the O1s spectra. In addition, it is again observed an increase in the carbon concentration, specifically of the C–C and C–O contribution for the data obtained at a smaller take-off angle (15°). At a small take-off angle the probing volume becomes more superficial and hence, a larger percentage of the volume corresponds to the adventitious contamination layer and consequently, the contribution related to the contamination layer becomes more important.

Table S3. Atomic concentration and standard deviation calculated from three independent measurements of each deconvoluted chemical state in the C1s and O1s photoelectron peaks.

Atomic concentration of each deconvoluted chemical state C1s and O1s peaks							
Oxide	**Take-off angle**	**C–C [at.%]**	**σ_{C-C} [at.%]**	**–OCO [at.%]**	**σ_{-OCO} [at.%]**	**–CO [at.%]**	**σ_{-CO} [at.%]**
SAA 45 °C	45°	13	2	1	0	1	0
SAA 45 °C	15°	15	1	1	0	2	0
SAA 37 °C	45°	14	1	1	0	2	0
SAA 37 °C	15°	17	1	1	0	2	0
TSA 55 °C	45°	9	1	2	1	3	1
TSA 55 °C	15°	11	1	1	1	3	0
TSA 37 °C	45°	14	1	1	0	1	1
TSA 37 °C	15°	21	0	1	1	2	1
T^+SA 55 °C	45°	14	2	1	1	2	0
T^+SA 55 °C	15°	18	2	1	0	2	1
T^+SA 37 °C	45°	12	1	1	0	2	0
T^+SA 37 °C	15°	15	0	1	0	2	0
Oxide	**Take-off angle**	**O_2 [at.%]**	**σ_{O2} [at.%]**	**$-OH^-$ [at.%]**	**σ_{-OH} [at.%]**	**H_2O [at.%]**	**σ_{H2O} [at.%]**
SAA 45 °C	**45°**	**40**	**3**	**11**	**2**	**1**	**1**
SAA 45 °C	15°	38	2	11	2	2	0
SAA 37 °C	45°	38	2	13	1	1	0
SAA 37 °C	15°	34	2	12	1	1	1
TSA 55 °C	45°	41	0	15	1	2	1
TSA 55 °C	15°	38	1	14	1	1	1
TSA 37 °C	45°	41	0	11	0	0	0
TSA 37 °C	15°	36	1	11	1	0	0
T^+SA 55 °C	45°	40	2	11	1	1	1
T^+SA 55 °C	15°	37	2	10	1	2	0
T^+SA 37 °C	45°	42	1	12	1	2	0
T^+SA 37 °C	15°	35	4	15	2	3	2

Taking into account the chemical composition of the oxides, as well as the results of the deconvolution of the detailed spectra, no evidence for the presence of tartrate in the TSA and T^+SA barrier oxide layers can be found in this data.

To study whether there are gradients in the chemical composition of the barrier anodic oxide films from the surface towards the oxide/substrate interface, XPS depth profiles have been measured. Therefore, the surface of the samples was sputtered by bombarding it with Ar^+ ion-clusters. The aggressiveness of the sputtering process can be controlled by the accelerating voltage applied between the sample surface and the Ar-cluster gun, as well as through adjusting the sputtering time between XPS spectra acquisition. As barrier oxide films are very thin, mild sputtering conditions have been chosen, meaning that only a few nanometers are sputtered away per cycle. A total of 50 min of sputtering were performed. As an example, the sputtering profiles of an SAA oxide anodised at 14 V and 45°C and of a TSA oxide anodised at 14 V and 55 °C are shown in Figure S3. From the profiles in Figure S3a and Figure S3b it can be derived that the SAA oxide (S3a) is thinner, as the anodic oxide/substrate interface is clearly reached after 50 minutes of sputtering while this is not the case for the TSA anodic oxide film (in Figure S3b). Furthermore, having a look at the elements present at low concentrations (<10%) similar sulfur content is measured for both oxides (ca. 1 at.%). On the contrary, the concentration of fluoride is higher in the case of the TSA anodic oxide. Fluoride is most likely coming from the fluoride-containing

acidic pickling pre-treatment bath. Finally, the presence of carbon is particularly interesting, as its presence in the oxide film could provide a hint of tartrate incorporation from the anodising electrolyte. However, carbon is also present due to adventitious contamination on the samples. Both SAA and TSA oxides (Figure S3a,b) show a rapid decrease of the carbon concentration, characteristic of the sputtering of the adventitious contamination layer. Although the presence of carbon in the TSA oxide seems to be slightly higher for longer sputtering times (11 minutes sputtering time compared to 20 minutes to reach concentrations below 0.1 at.%), this is most likely due to small differences in the thicknesses of the contamination layer. Consequently, no evidence can be extracted that points toward the presence or incorporation of tartrates into the barrier anodic oxide films.

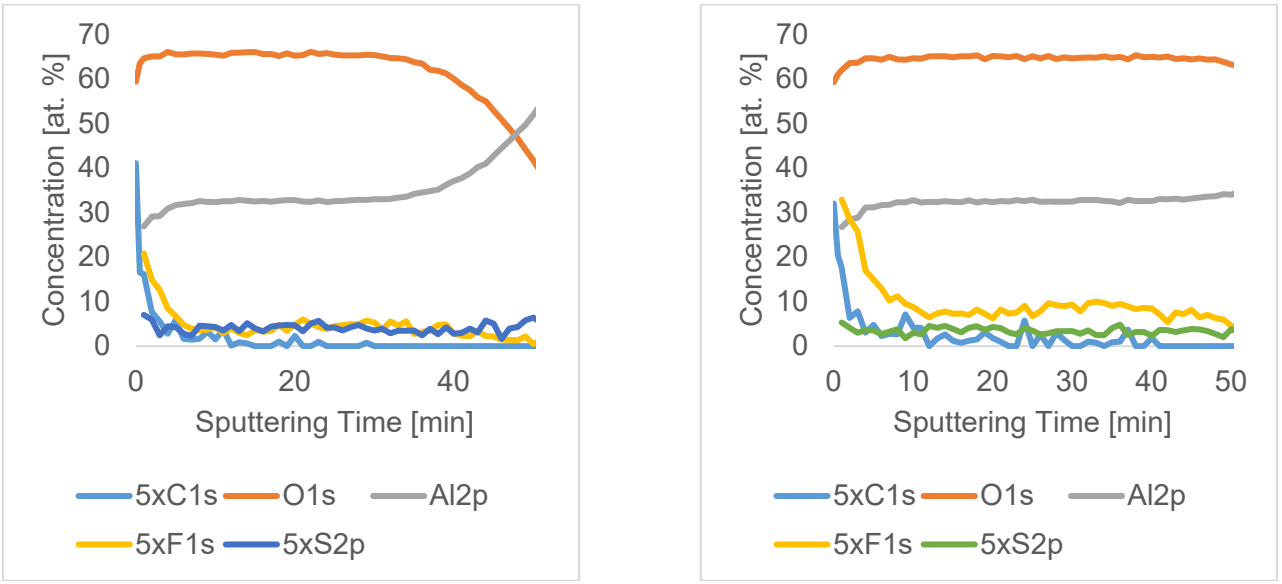

Figure S3. Depth profile of barrier oxide films. (**a**) SAA 14 V 45 °C; (**b**) TSA 14 V 55 °C. Concentration of C, F and S multiplied by 5.

2.1.2. XPS Characterisation of Porous Layers

Detailed spectra of the elements identified in the survey scan were measured (Figure S4), and an estimation of the chemical composition was performed based on the detailed spectra (Table S4).

The shape of the C1s and O1s spectra (Figure S4a) and b)) is very similar for all six oxides. This again means, that no clear evidence could be found that indicates tartrate incorporation, at least not in the near-surface area of the porous anodic oxide film. A higher intensity and estimated concentration of fluoride (Figure S4d)), present due to the acidic pickling process step in a fluoride containing solution, has been observed in the oxides formed at lower anodising temperatures. In addition, the F1s peak shifts to higher binding energies (ca. 686.3 vs 685.3 eV) in the case of oxides formed at 20 V and 37 °C. Among oxides formed in the same temperature range, a higher concentration is observed in oxides formed in an electrolyte with a high tartaric acid concentration, followed by the intermediate tartaric acid concentration and finally the SAA oxide.

A consistent trend is also observed in the case of the signal intensity and consequently the estimated chemical composition of the S2p photoelectron peak (Figure S4c)), with higher intensities for the oxides formed at lower electrolyte temperatures.

As it was previously mentioned, the quantification of the chemical composition of porous anodic oxide films should be carefully considered, as the measurement of mixed signals and the increased roughness and porosity of the oxides formed at elevated temperature add to the differences observed in the fluoride and sulfur signal intensities.

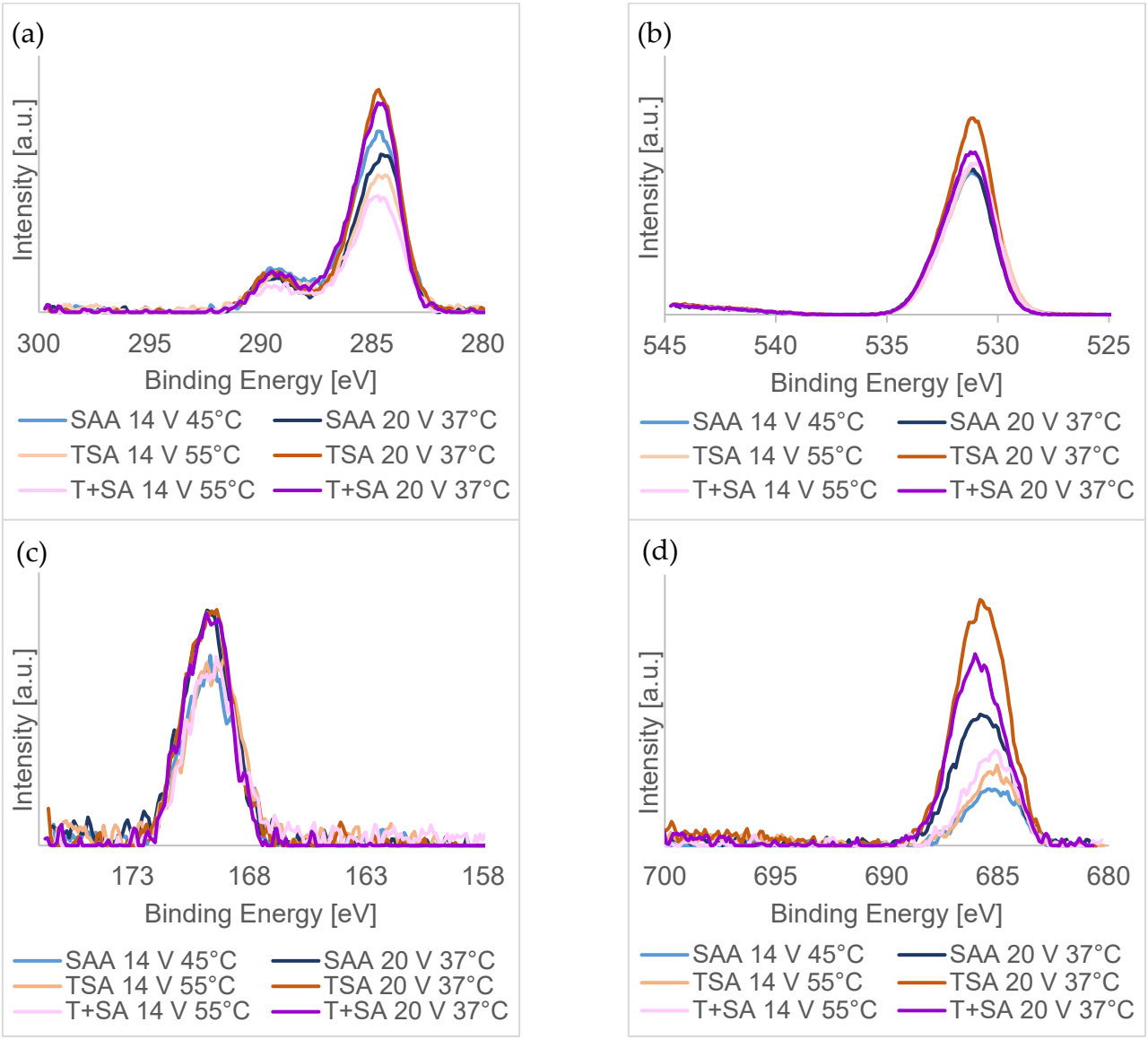

Figure S4. Detailed Spectra Porous Layer of (**a**) C1s; (**b**) O1s; (**c**) S2p; (**d**) F1s.

Table S4. Chemical composition estimated from the detailed spectra of porous anodic oxide films.

Oxide	C1s [at.%]	σ_{C1s} [at.%]	O1s [at.%]	σ_{O1s} [at.%]	F1s [at.%]	σ_{F1s} [at.%]	Al2p [at.%]	σ_{Al2p} [at.%]	S2p [at.%]	σ_{S2p} [at.%]
SAA 14 V 45 °C	6.8	0.1	59.6	0.6	1.9	0.3	30.1	0.3	1.7	0.1
SAA 20 V 37 °C	5.1	0.4	58.3	0.1	4.4	0.4	30.2	0.2	2.1	0.2
TSA 14 V 55 °C	5.5	0.5	59.8	0.3	2.4	0.4	30.7	0.1	1.5	0.2
TSA 20 V 37 °C	6.8	0.9	56.5	0.1	4.8	0.4	30.3	0.6	1.7	0.1
T+SA 14 V 55 °C	5.9	1.6	59.2	1.0	2.5	0.0	30.7	0.6	1.7	0.1
T+SA 20 V 37 °C	7.3	1.2	55.8	0.8	5.2	0.3	29.8	0.6	1.8	0.0

2.2. Oxide chemistry characterisation by ToF-SIMS

2.2.1. Barrier Oxide Layers

The chemistry of some of the barrier anodic oxide films, in particular those formed in SAA, TSA and T+SA at 37°C, were further studied by ToF-SIMS.

Figure S5 shows the spectra measured corresponding to the tartrate molecule fragment $C_4H_5O_6^-$. Although counts are detected, this is most likely coming from the organic

contamination layer on the surface, as the signal measured is very similar for all three oxides (SAA, TSA and T⁺SA), regardless of the presence or absence of tartaric acid in the anodising electrolyte. In addition, the intensity of the signal is relatively low, two orders of magnitude lower than the intensity measured for SO_2^- (not shown).

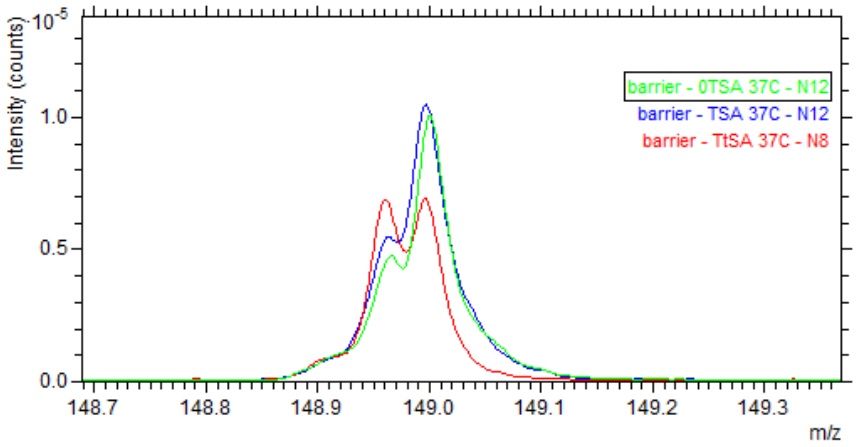

Figure S5. ToF-SIMS spectra of $C_4H_5O_6^-$ molecular fragment measured on SAA, TSA and T⁺SA barrier anodic oxides films formed at 37°C.

2.2.2. Porous Oxide Layers

The chemical composition of SAA, TSA and T⁺SA porous anodic oxide films formed at 37°C were also studied by ToF-SIMS.

Figure S6 shows the spectra obtained corresponding to a protonated tartrate molecular fragment and an aluminium tartrate molecular fragment (Figure S6a and Figure S6b) respectively). No signal for these two particular molecular fragments was detected in barrier oxide layers. The higher intensity measured for TSA and T⁺SA could be interpreted as a presence of tartaric acid remnants or as the adsorption of tartrates on the oxide surface. However, due to the fact that tartrate species can also be found in SAA samples, further investigation would be needed to confirm if this signal is really coming from electrolyte remnants or if it is caused by the adventitious contamination.

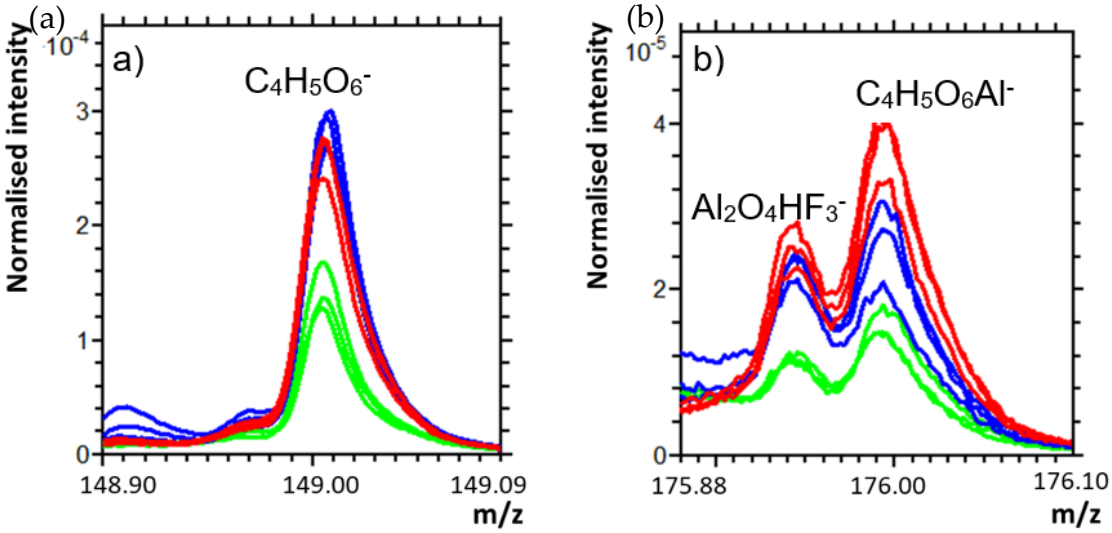

Figure S6. ToF-SIMS spectra of a protonated tartrate molecular fragment ($C_4H_5O_6^-$) (**a**) and (**b**) of an aluminum tartrate molecular fragment ($C_4H_5O_6Al^-$). Measured on SAA, TSA and T⁺SA porous oxide films formed at 37 °C.

In agreement with what was observed in the XPS spectra, a higher intensity of fluoride (Figure S7) is measured for TSA and T⁺SA compared to SAA porous anodic oxides.

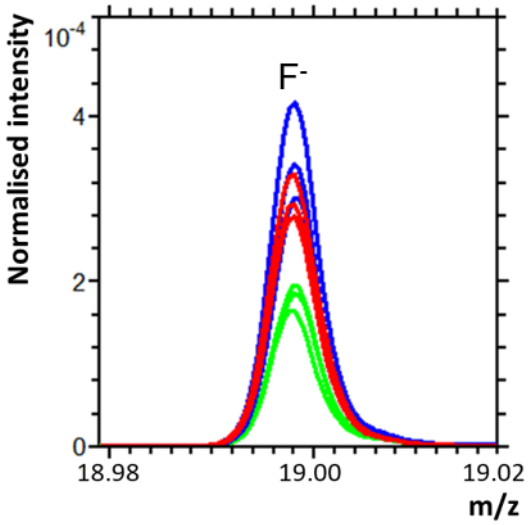

Figure S7. ToF-SIMS spectra of F^- molecular fragment. Measured on SAA, TSA and T⁺SA porous oxide films formed at 37 °C.

3. Oxide Chemistry Characterisation: Discussion

The only relevant difference in chemical composition among the studied oxides is the higher fluoride concentration of TSA and T⁺SA oxides measured by both XPS and ToF-SIMS. The source for fluorides is the acidic pickling operation prior to anodising, as they are added to the pickling solution to shorten the process and lower the bath temperature [2]. After acidic pickling, a residual pickling oxide is found on the substrate surface, which contains elements from the pickling solution e.g., fluorides. During anodising, unless the oxide dissolution reaction at the electrolyte/oxide interface is strong enough to (completely) dissolve the pickling oxide, it will remain present on the surface, as the oxide growth during anodising takes place at the oxide/substrate interface. In addition, in the presence of the anodising electric field, fluoride ions can migrate from the electrolyte/oxide interface towards the oxide/substrate interface [3]. This ionic migration explains the presence of fluorides in the bulk anodic oxide film. Taking into account the origin of fluorides, the higher fluoride concentration of TSA and T⁺SA oxides can be explained by the reduced aggressiveness of the mixed electrolyte compared to SAA [4], which translates into a milder oxide dissolution reaction, and therefore into a higher retention of the fluoride containing pickling oxide.

Besides the differences in intensity, the F1s detailed photoelectron spectra also reveals a shift towards higher binding energies for the oxides formed at lower temperature and higher formation voltages. The higher binding energy (686.3) is characteristic of $AlF3{\cdot}3H_2O$ [5], while the lower binding energy (685.3) is closer to reported characteristic binding energies of AlF6 [6].

References

1. Abrahami, S.T.; Hauffman, T.; de Kok, J.M.; Mol, J.M.; Terryn, H. XPS Analysis of the Surface Chemistry and Interfacial Bonding of Barrier-Type Cr(VI)-Free Anodic Oxides. *J. Phys. Chem. C* **2015**, *119*, 19967–19975. https://doi.org/10.1021/acs.jpcc.5b05958.
2. Carangelo, A.; Curioni, M.; Acquesta, A.; Monetta, T.; Bellucci, F. Cerium-based sealing of anodic films on AA2024T3: effect of pore morphology on anticorrosion performance. *J. Electrochem. Soc.* **2016**, *163*, C907–C916.
3. Elaish, R. Effects of fluoride ions in the growth of barrier-type films on aluminium. *Electrochim. Act.*, **2017**, *245*, 854–862, doi:10.1016/j.electacta.2017.06.034.
4. Paz Martínez-Viademonte, M.; Abrahami, S.T.; Hack, T.; Burchardt, M.; Terryn, H. Adhesion properties of tartaric sulfuric acid anodic films assessed by a fast and quantitative peel tape adhesion test. *Int. J. Adhes. Adhes.* **2022**, *116*, 103156

5. Moulder, J.F.; Chastain, J. Handbook of X-ray Photoelectron Spectroscopy: A Reference Book of Standard Spectra for Identification and Interpretation of XPS Data; Physical Electronics Division, Perkin-Elmer Corporation: Waltham, MA, USA, 1992.
6. Limcharoen, A.; Pakpum, C.; Limsuwan, P. An X-ray Photoelectron Spectroscopy Investigation of Redeposition from Fluorine-based Plasma Etch on Magnetic Recording Slider Head Substrate, *Proc. Eng.* **2012**, *32*, 1043–1049.